

Full length article

Performance-based seismic design of staggered truss frames with friction dampers

Jinkoo Kim^{*}, Soyeon Kim

Department of Civil and Architectural Eng., Sungkyunkwan University, Suwon, Republic of Korea

ARTICLE INFO

Keywords:

Capacity design
Staggered truss
Friction dampers
Fragility analysis

ABSTRACT

In this study performance-based seismic design procedure for staggered truss frames with friction dampers in the vierendeel panels was developed and their seismic performance was evaluated. To this end 6- and 12-story analysis model structures with friction dampers were designed using the capacity design procedure. For comparison the same structures without dampers were designed following the strength based approach specified in the ASCE 7–13, and the seismic performances of all model structures were compared. Fragility analyses were carried out to evaluate the seismic safety of the model structures and to validate the response modification factor used for seismic design. Analysis results showed that the capacity design method led to the formation of plastic hinges concentrated at vierendeel panels. It was also observed that the substitution of rotational friction dampers at the location of plastic hinges resulted in enhanced ductility and reduced probability of failure when the structures were subjected to design level seismic load.

1. Introduction

The staggered-truss frames (STF) consist of a series of story-high trusses spanning the total width between exterior columns on the opposite sides of the building and arranged in a staggered pattern on adjacent column lines. The STF has the advantage that large clear span and open areas are possible because columns are located only on the exterior faces of the building. As story-high staggered trusses function as floor beams as well as partition walls, story height can be minimized and significant advantage in economy can be achieved. It is also reported that the structural costs per unit building area is relatively low in staggered-truss framed structures [1]. Staggered truss systems have been successfully applied to many large-scale building projects and their efficiency and economy are reported [2]. Kim et al. [3] conducted nonlinear static analyses of staggered truss system buildings and identified failure modes under seismic loads. Zhou et al. [4] conducted a series of experimental and numerical analysis on the seismic behavior of staggered truss systems, and investigated the influence of the typical design parameters. Chen and Zhang [5] and Chen et al. [6] carried out experimental research to study the failure mode and joint capacity of a steel staggered truss system model exposed to pool fire. Kim et al. [7] proposed various seismic retrofit schemes for STF without and with vierendeel panels, and showed their validity through fragility analysis. Recently similar design concept utilizing vertically staggered wall panels was applied to design of reinforced

concrete structures [8].

The staggered truss frames, however, have not been considered as one of the basic seismic-force-resisting systems in design codes, which implies that further research is still necessary for the system to be accepted as a standard structure system for seismic load. It is specified in the FEMA-450 [9] that a seismic-force-resisting systems that are not listed as the basic seismic-force-resisting systems can be permitted if analytical and test data are submitted to demonstrate the lateral force resistance and energy dissipation capacity. To facilitate the application of the STF, AISC (American Institute of Steel Construction) published the Design Guide 14: Staggered Truss Framing Systems [10], in which some recommendations and examples for structural design are provided.

These days various energy dissipation devices are widely used in order to improve the seismic behavior of structures. Morgen and Kurama [11] carried out a seismic response evaluation tests of unbonded posttensioned precast concrete moment frames with friction dampers at selected beam ends. Chung et al. [12] proposed a friction damper that is applied between coupled shear walls in order to reduce the deformation of the structure induced by earthquake loads. Mualla et al. [13] developed a rotational friction damper which can produce maximum friction force as high as 5000 kN, which was later applied to the Abeno Harukas Building in Japan [14,15]. Dai et al. [16] developed electromagnetic friction dampers for seismic energy dissipation of building structures. Currently in Korea rotational friction dampers are

^{*} Corresponding author.

E-mail address: jkim12@skku.edu (J. Kim).

used in link beams connecting coupled shear walls as an alternative of deep link beams congested with diagonal and transverse rebars.

This study is focused on the validation of the effectiveness of rotational friction dampers for seismic design of staggered truss frames. The performance based seismic design is applied on steel staggered truss systems with friction dampers installed in the chord members of vierendeel panels, and their seismic performance and fragility are evaluated. To this end, 6- and 12-story structures with friction dampers are designed based on the capacity design procedures. The same structures without dampers are designed following the conventional strength-based procedure specified in the ASCE 7–13 [17], and the seismic performances of all model structures are compared. Fragility analyses are carried out using 44 earthquake ground records to evaluate the seismic safety of the model structures and to validate the response modification factor used for seismic design of staggered truss systems.

2. Design of model structures

2.1. Design of conventional staggered truss systems

As conventional STF analysis model structures, 6- and 12-story buildings are designed using the design loads specified in the ASCE 7–13. The staggered trusses are located along the transverse direction, and the moment-resisting frames are placed along the longitudinal direction. Along the transverse direction, the staggered trusses and the perimeter columns are connected by pin joints, and columns and perimeter beams are rigidly connected along the longitudinal direction. No truss is placed in the first story to accommodate large open space; instead diagonal members are installed at both ends of the span along the transverse direction as is done in the example structure of the AISC Steel Design Guide [10]. Along the transverse direction a 2 m long vierendeel panel without a diagonal member is located in the middle of two staggered trusses, which is generally used as a corridor. In each staggered truss, story-high vertical elements are located in the interval of 3 m, and a diagonal member is placed between two vertical members. Fig. 1 depicts the three dimensional view and structural plan of the 6-story analysis model structure. The staggered arrangement of the floor-deep trusses placed at alternate levels on adjacent column lines allows an interior floor space of twice the column spacing to be available for freedom of floor arrangements. The floor system spans from the top chord of one truss to the bottom chord of the adjacent truss, serving as a diaphragm transferring the lateral shears from one column line to another. This enables the structure to perform as a single braced frame, even though the trusses lie in two parallel planes. With the columns only on the exterior walls of the building, the usual interior columns are omitted, thus providing a full width of column-free area on the first floor. Exterior columns are located in such a way that their

strong axes are in parallel with longitudinal direction of the structures as recommended in the Design Guide. The columns and beams are rigidly connected along the longitudinal direction, and the staggered trusses and the columns are pin connected as shown in Fig. 1(b). The height of the typical stories is 3 m and the height of the first-story is set to be 4 m. The column spacing along the longitudinal direction is 9 m.

The design loads for the model structures are determined based on the ASCE 7–13 and structural member design is carried out based on the Load and the Resistance Factor Design (LRFD) of AISC [18]. The dead load is estimated to be 5.0 kN/m² and live load of 2.0 kN/m² is used assuming that the structures are used as residential buildings. Along the transverse direction, where staggered trusses are located, the response modification factor of 3.0 is applied in the computation of the seismic design base shear, which is generally applied in structural steel systems not specifically detailed for seismic resistance; along the longitudinal direction, where the seismic force-resisting system is the ordinary moment-resisting frames, the response modification factor of 3.5 is used as recommended in the design code. The design spectral acceleration parameters for short period (S_{DS}) and at 1.0 s (S_{D1}) are assumed to be 1.0 and 0.6, respectively, and the short- and the long-period site coefficients F_a and F_v are 1.0 and 1.5, respectively, in the ASCE 7-13 format. The site class is assumed to be D, and the design spectral acceleration parameters correspond to the seismic design category D. These assumptions lead to seismic design loads similar to those for structures located in San Francisco area with the same site class.

Structural analysis and design of the model structure is carried out using the general purpose software MIDAS-Gen [27]. In all model structures, columns and upper and lower chords of the staggered truss are designed with A572M steel ($F_y = 345$ MPa, $F_u = 450$ MPa) and the other members are made of A500M steel ($F_y = 250$ MPa, $F_u = 400$ MPa). The columns are designed in such a way that the demand/strength ratio is about 0.8 and the other members around 0.9. The 20 cm thick floor slabs, which is designed to resist gravity load as well as the inplane shear force transmitted from the staggered truss located above, are assumed to be a rigid diaphragm in structural analysis. According to the modal analysis, the fundamental natural period of the 6-story model structure is 1.50 and 0.56 s for the longitudinal (moment frame) and the transverse (staggered truss) directions, respectively. Those of the 12-story structure turned out to be 1.81 and 0.78 s, respectively. It can be noticed that the natural periods along the transverse direction, where staggered trusses are located, are significantly smaller than those along the longitudinal direction. The fundamental vibration mode shapes of the structures are depicted in Fig. 2, where the mode shapes of the structures along the transverse direction are similar to those of a typical moment resisting frame, due to the flexural deformation of the vierendeel panel.

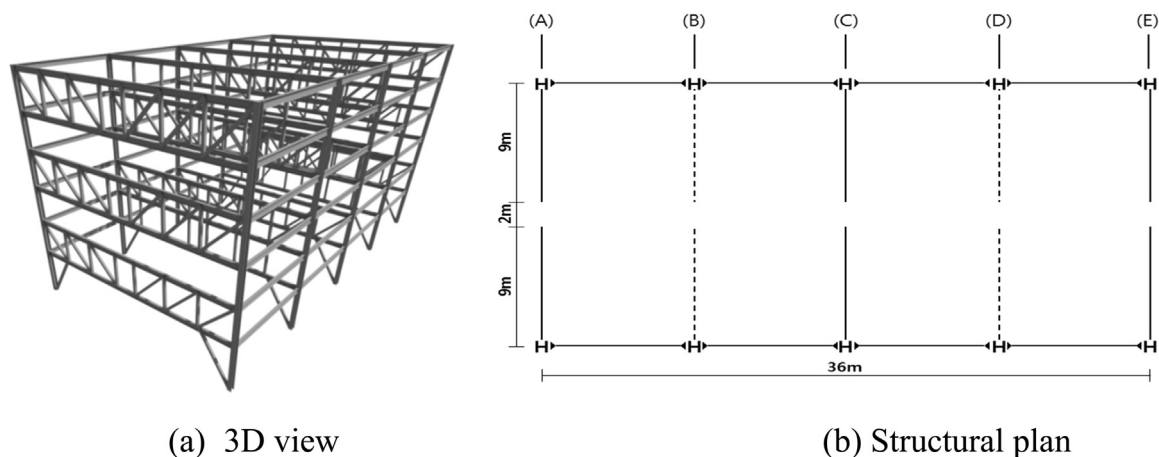


Fig. 1. Analysis model structure (6-story). (a) 3D view (b) Structural plan.

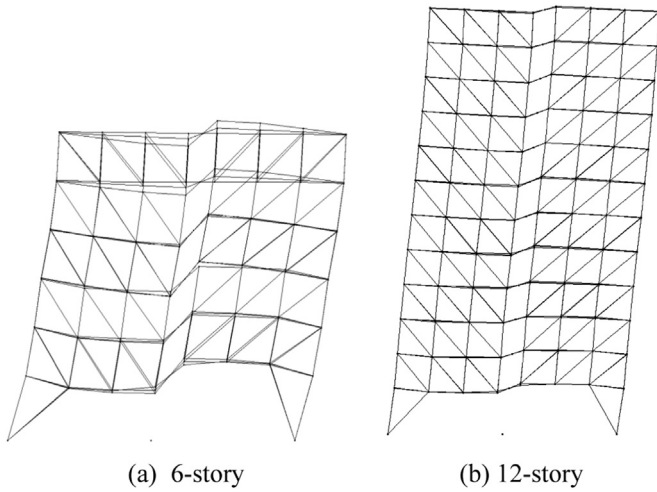


Fig. 2. Fundamental mode shapes of the model structures. (a) 6-story (b) 12-story.

2.2. Capacity design of model structures with friction dampers

The objective of capacity design is to confirm controlled ductile behavior of structures in order to avoid collapse in a design-level earthquake. This involves designing the structure to allow ductile failure at key predictable locations within the structure and to prevent other failure types which may lead to unpredictable brittle failure. In this study the concept of capacity design is realized using rotational friction dampers which can be manufactured to have larger deformation and energy dissipation capacity than those of typical plastic hinges formed at beam ends. With rotational friction dampers at the ends of vierendeel panels, a capacity design procedure is applied to lead the formation of plastic hinges localized in the vierendeel panels and to maximize the energy dissipation in the dampers. To ensure yielding of dampers prior to other structural elements, the structures are designed in such a way that the plastic hinges are concentrated at the vierendeel panels and the other members remain elastic. In the event of design level earthquakes, only the damaged friction dampers can be replaced. Similar approach is successfully applied to the design of special truss moment frames by Chao and Goel [19], who designed the special segment in the floor truss girders using the plastic design. In their approach the other structural members outside the special segments are designed based on the capacity design approach so that they remain elastic during seismic events.

The capacity design of the staggered truss systems starts from the design of the chord members of the vierendeel panels based on their required flexural strength at the ends. The target deformation shape and plastic hinge formation is depicted in Fig. 3. The required bending capacity of a plastic hinge formed at the end of the vierendeel panel at the i^{th} story, M_{pi} , can be calculated from the following equilibrium equation of the internal and external works [19]:

$$\sum_{i=1}^n F_i h_i \theta_p = 2M_{pc} \theta_p + 2 \sum_{i=1}^n M_{pi} \frac{L}{L_v} \theta_p \quad (1)$$

where F_i is the equivalent seismic load obtained using the vertical seismic force distribution method in the ASCE 7-13, h_i is the height from the ground to the i^{th} story, M_{pi} is the required plastic moment of a vierendeel panel chord member in Level i , M_{pc} is the required plastic moment of a column in the first story, L is the span length of staggered truss, L_v is the length of the chord member of the vierendeel panel, and θ_p is the given target drift angle. In the above equation the lateral seismic force and the geometric information of the model structure are given values and the moment capacities of the columns and the chord members of the vierendeel frame are to be determined. Assuming that plastic hinges form at the base and top of the first story columns, the

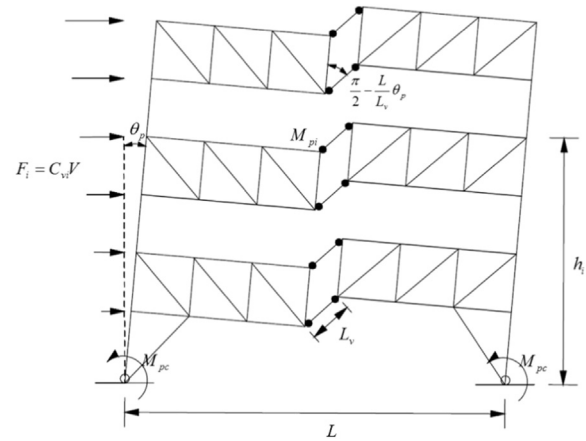


Fig. 3. Desired deformed configuration and location of plastic hinges when subjected to lateral load.

moment capacity of the first story columns, M_{pc} , can be obtained from the equivalence of the external and internal works as follows [19]

$$M_{pc} = \frac{R_y V h_1}{4} \quad (2)$$

where V is the base shear, h_1 is the height of the first story; and R_y is the over strength factor specified in the AISC Seismic Provisions for Structural Steel Buildings [20] which is 1.1. Eq. (1) can be rewritten as follows to obtain the total moment capacities of the chord members in the vierendeel panel:

$$\sum_{i=1}^n M_{pi} = \frac{\sum_{i=1}^n F_i h_i - 2M_{pc}}{2 \frac{L}{L_v}} \quad (3)$$

In this study the total moment capacity of the chord members is distributed to each story proportional to the seismic story shear as follows:

$$M_{pi} = \frac{V_i}{\sum_{i=1}^n V_i} \sum_{i=1}^n M_{pi} \quad (4)$$

where V_i is the story shear in level i . The chord members in each story can be designed from the required moment capacity of each chord member determined above using the resistance factor of 0.9.

Fig. 4(a) shows the free body diagram of the left half of the staggered truss structure when all chord members yield. To concentrate the plastic hinges at the vierendeel panel when subjected to seismic load, the elements outside the vierendeel panel should be designed to resist the combination of factored gravity loads and the maximum vertical shear force developed at the vierendeel panel, V_p , which is obtained as follows:

$$V_p = \frac{2R_y M_n}{L_v} \quad (5)$$

where M_n is the nominal moment strength of the chord. Table 1 shows the size and moment capacities of the chord members and the maximum vertical shear force developed at each chord member, V_p , at the exterior frame A depicted in Fig. 1(b). At this stage the first story columns are also assumed to have reached their maximum capacity. When the lateral forces are applied to the right as shown in Fig. 4(a), the required balancing lateral forces applied on this free body can be obtained as follows using the moment equilibrium:

$$\sum_{i=1}^n (F_L)_i h_i + \frac{L^2}{8} \sum_{i=1}^n w_{iu} = \frac{L}{2} \sum_{i=1}^n (V_p)_i + M_{pc} \quad (6)$$

The moment equilibrium equation for the right half of the model structure can be similarly obtained. From above equation the required

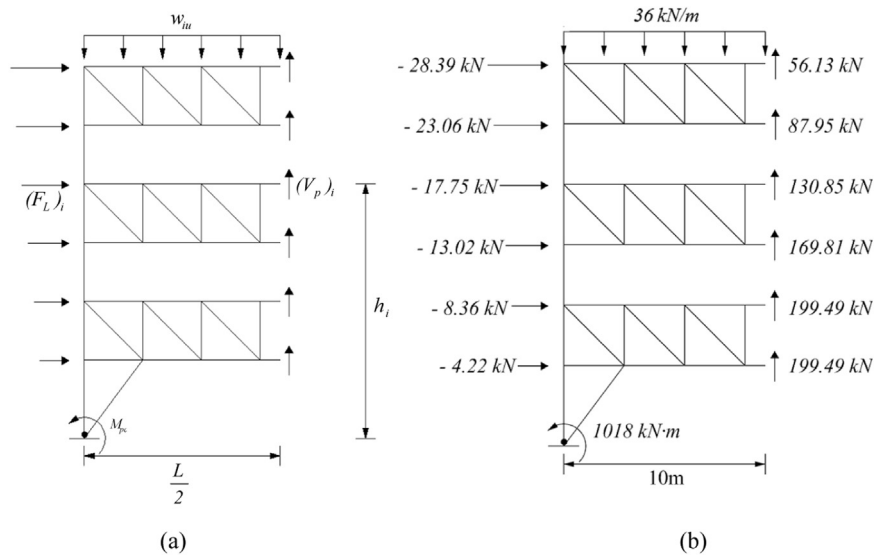


Fig. 4. Design loads for the structural members other than the chord members of the vierendeel panel.

Table 1
Size, moment capacity, and the maximum shear force of the chord members (Line A).

Story	Section	M _{nc} (kN m)	V _p (kN)
6	H 148 × 100 × 6/9	51	56.13
5	H 150 × 150 × 7/10	80	87.95
4	H 250 × 125 × 6/9	119	130.85
3	H 298 × 149 × 5.5/8	154	169.81
2	H 244 × 175 × 7/11	181	199.49
1	H 244 × 175 × 7/11	181	199.49

balancing lateral forces for the left and the right half parts can be obtained as follows:

$$\sum_{i=1}^n (F_L)_i = \frac{\frac{L}{2} \sum_{i=1}^n (V_p)_i - \frac{L^2}{8} \sum_{i=1}^n w_{iu} + M_{pc}}{\sum_{i=1}^n h_i} \quad (7a)$$

$$\sum_{i=1}^n (F_R)_i = \frac{\frac{L}{2} \sum_{i=1}^n (V_p)_i + \frac{L^2}{8} \sum_{i=1}^n w_{iu} + M_{pc}}{\sum_{i=1}^n h_i} \quad (7b)$$

In this study the total lateral forces obtained from Eq. (7) are vertically distributed using the vertical distribution factor specified in the ASCE 7-13. The seismic story forces acting on the left- and right-hand side free bodies used to design the members outside the vierendeel panel are obtained as follows:

$$(F_L)_i = C_{vi} \sum_{i=1}^n (F_L)_i \quad (8a)$$

$$(F_R)_i = C_{vi} \sum_{i=1}^n (F_R)_i \quad (8b)$$

The vertical distribution factor at level *x*, *C_{v_x}*, specified in the ASCE 7-13 is given by

$$C_{vx} = \frac{w_x h_x^k}{\sum_{i=1}^n w_i h_i^k} \quad (9)$$

where *w_x* is the effective seismic weight of the structure at level *x*, *h_x* is the height from the base to level *x*, and *k* is an exponent related to the structure period. For the 6- and the 12-story structures along the transverse direction, *k* is 1.03 and 1.14, respectively. The structural elements outside of the vierendeel panel are designed to respond elastically for the gravity loads and the lateral load computed above. Fig. 4(b) shows the numerical values for the factored gravity load, the

maximum vertical shear forces developed at the chord members of the vierendeel panel, and the required balancing lateral forces acting on the free body. The structural design is completed by inserting friction dampers at both ends of the chord members in the vierendeel panel, as shown in Fig. 5, with their moment capacities equal to those of the chord members determined by Eq. (4). The insertion of rotational friction dampers significantly increases the rotational capacity of the chord members in the vierendeel panels.

3. Nonlinear analysis of the model structures

3.1. Nonlinear static analysis results

Nonlinear static analyses of the model structures designed without and with friction dampers at the vierendeel panel are carried out to evaluate the seismic performance of the model structures. The nonlinear force-deformation relationships of structural members recommended in the ‘Seismic Evaluation and Retrofit of Existing Buildings’ (ASCE/SEI 41-13) [21], shown in Fig. 6, are used in the analysis. The limit states of IO (Immediate Occupancy), LS (Life Safety), and CP (Collapse Prevention) are indicated on the curves. The specified limit states vary depending on the factors such as width-thickness ratio for beams and columns and the axial force for columns. Table 2 shows the

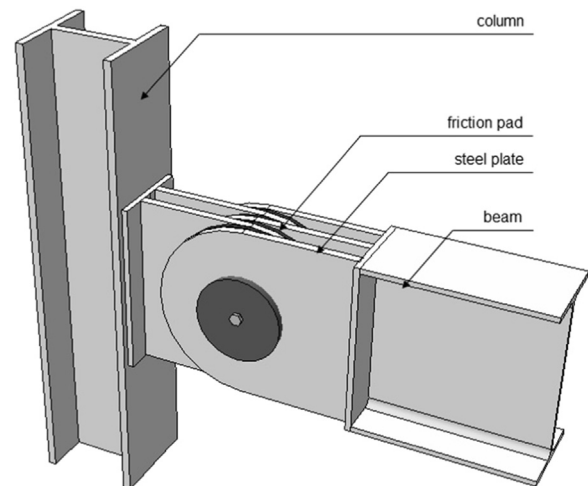


Fig. 5. Configuration of a rotational friction damper installed at the ends of chord members of vierendeel panel.

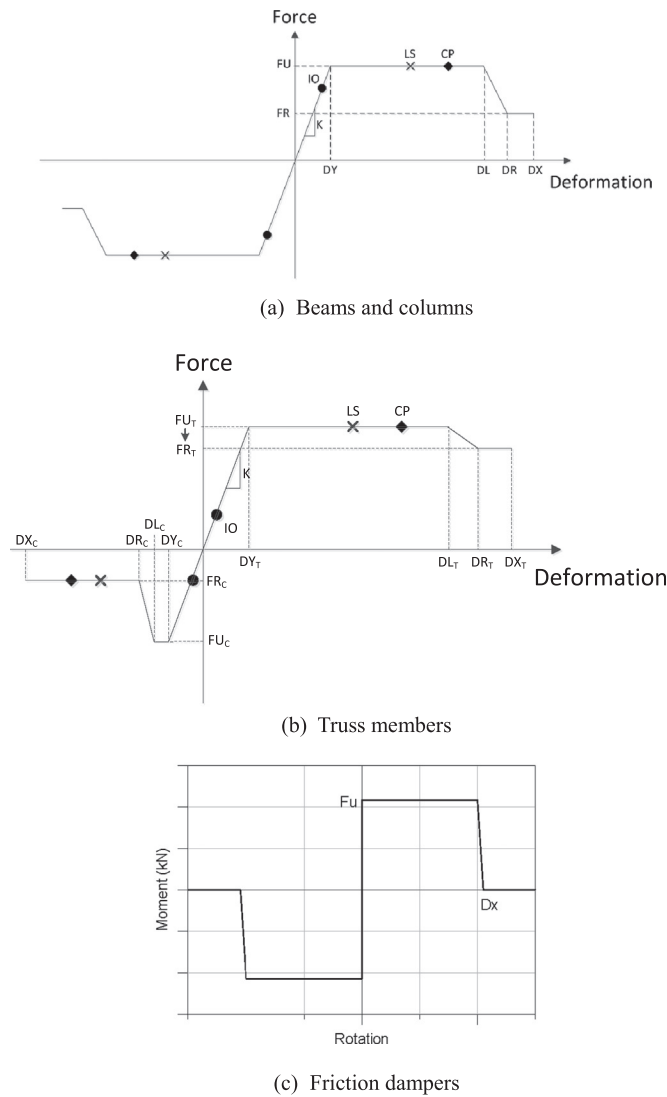


Fig. 6. Force-deformation relationships for structural elements used in the analysis. (a) Beams and columns, (b) Truss members, (c) Friction dampers.

Table 2
Limit states for first story columns and chord members of the strength-designed 6-story structure.

	IO	LS	CP
Columns	$0.25\theta_y$	$0.5\theta_y$	$0.8\theta_y$
Chords	$1\theta_y$	$6\theta_y$	$8\theta_y$

limit states for the first story columns and chord members of the strength-designed 6-story structure. The failure point of the rotational friction dampers at which the friction force starts to be lost is conservatively assumed to be 0.2 rad based on the experimental results of rotational friction dampers [22]. The nonlinear analysis software Perform 3D [23] is used for nonlinear analysis of the model structures.

Fig. 7 shows the base shear vs. roof displacement relationship of the model structures obtained from pushover analysis. The vertical lateral load profile is obtained from the fundamental mode shapes of the structures. The design base shear and the roof displacements at the maximum inter-story drift of 2% and 4% of the story height are also indicated in the figure. It can be observed that, even though the two structures are designed for the same seismic load, the maximum strength of the structure designed following the strength-based approach is higher than that of the structure with dampers designed using

the capacity design approach. The ductility of the structure with the friction dampers, however, is much higher than that of the structure without dampers. In the structure with friction dampers the strength of the structure is maintained until the maximum inter-story drift of 0.2% is reached. It is also observed in the conventional structure that, right after the design base shear is reached, the first story chord member of the vierendeel panel in the Line C frame yields first. At point α in Fig. 7(a) the strength drops rapidly due mainly to the complete strength loss of the first story chord member in the Line A frame. In columns plastic hinge forms first at the first story column in Line B frame at the roof story displacement of 12 cm. In the structure with friction dampers, yielding of the structure occurs due to yielding of the friction dampers located in the lower stories right after the design base shear is reached. At the roof story drift of 15 cm, plastic hinge forms in the first story column. It is also observed that strength drops abruptly at point β when the rotation of the friction dampers located in the lower two stories reach the limit state of 0.2 rad.

Fig. 8 shows the plastic hinge formation in the three transverse rows of the strength-designed 6-story structure when the maximum inter-story drift reached 2% of the story height. It can be observed that plastic hinges form not only at the chord members in the vierendeel panel but also at the neighboring braced panels, and that they form mainly at the lower stories. Plastic hinges also form in the first story columns in all three frames and in the fourth story column in the frame B. Fig. 9 shows the plastic hinge formation at the two transverse rows of the capacity designed structure with friction dampers at the maximum inter-story drift of 2%. It can be observed that plastic hinges form at the first story columns and at the lower story friction dampers located in the vierendeel panel. No plastic deformation is observed in the chord and the diagonal members outside of the vierendeel panel, which confirms the validity of the capacity design applied.

Fig. 10 depicts the pushover analysis results of the 12-story structures. As in the 6-story structures, the strength-designed structure shows higher strength but lower ductility than the capacity-designed structure with friction dampers. It is observed that plastic hinges first form at the lower story chord members and then at the first story columns. Right after the maximum strength is reached (point γ in Fig. 10(a)), some diagonal members in the second story staggered trusses buckle, which leads to the major strength loss. In the structure with friction dampers the major strength loss occurs after the maximum inter-story drift ratio of 2% is exceeded. The strength drop (at point δ in Fig. 10(b)) is caused by the failure of the friction dampers located below the fifth story. Fig. 11 depicts the plastic hinge formation in the conventional strength-designed 12-story structure at the maximum inter-story drift ratio of 2%. It can be observed that many plastic hinges form at the chord members of the vierendeel panels and at the nearby braced panels. In addition, plastic hinges form at the first story columns and some diagonal and vertical members in the lower stories buckle under compression.

3.2. Nonlinear dynamic analysis results

In this section the seismic performances of the structures designed without and with friction dampers are compared using nonlinear dynamic analyses. Table 3 shows the lists of earthquake records used in the dynamic analysis selected from the PEER NGA Database [24]. They are scaled in such a way that their spectral accelerations corresponding to the fundamental natural periods of the model structures are equal to those of the design spectral values. Fig. 12 depicts the roof displacement time histories of the 6-story model structures subjected to the Imperial Valley earthquake, where it can be observed that, compared with the model structure designed using the strength based method, both the maximum displacement and the residual displacement decrease in the structure designed using the capacity design method with friction dampers. Fig. 13 shows the maximum inter-story drift ratios of the 6-story model structures. It

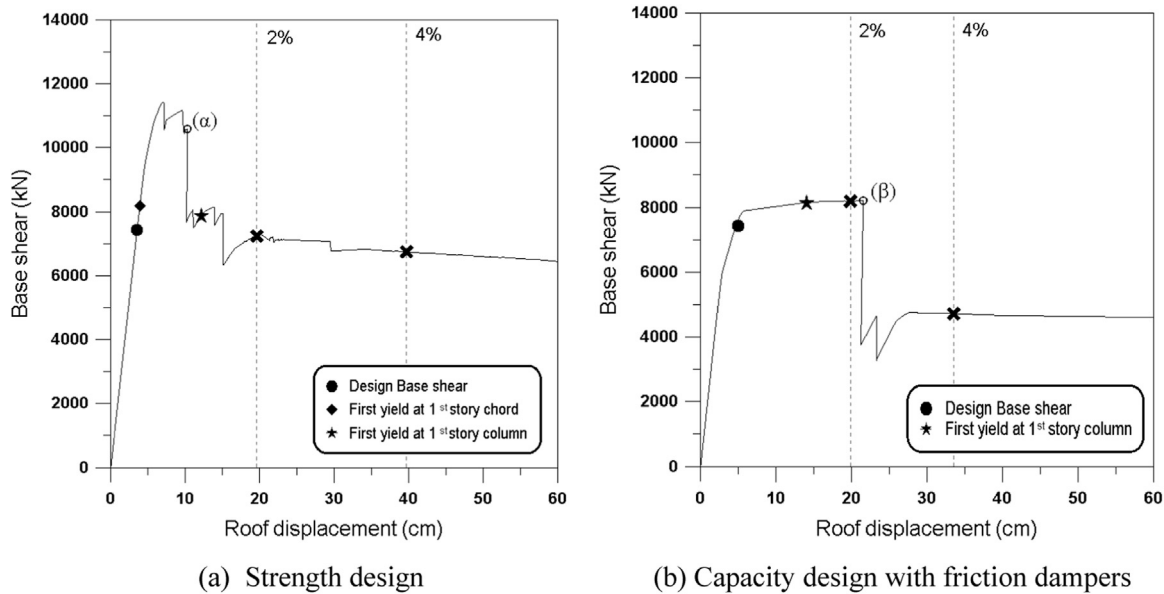


Fig. 7. Pushover curves of the 6-story structures. (a) Strength design, and (b) Capacity design with friction dampers.

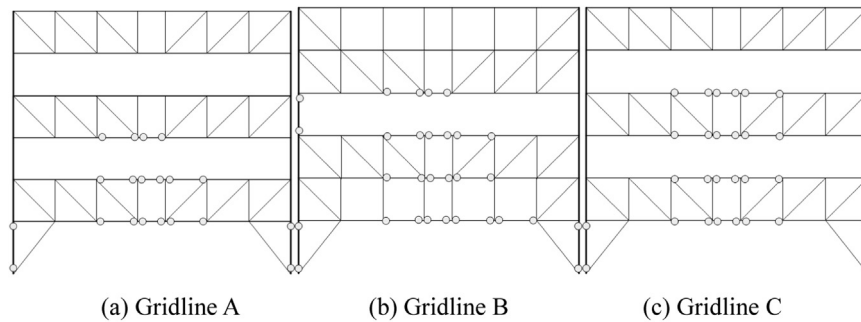


Fig. 8. Plastic hinge formation in the 6-story structure (Strength design). (a) Gridline A, (b) Gridline B, and (c) Gridline C.

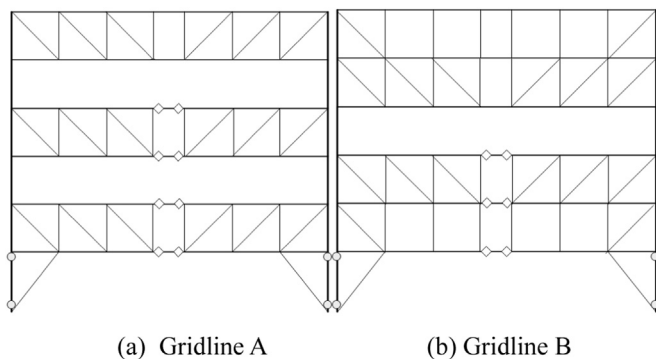


Fig. 9. Plastic hinge formation in the 6-story structure with friction dampers. (a) Gridline A, and (b) Gridline B.

can be observed that the maximum inter-story drifts of all structures are less than the limit state of 1.5% of the story height, and that the structures with friction dampers show smaller inter-story drifts. Fig. 14 depicts the plastic hinge formation in the strength-designed 6-story structure, which is similar to the plastic hinge formation obtained by the pushover analysis except that no plastic hinge is observed in the first story columns. Fig. 15 compares the dissipated energy in the 6-story model structures subjected to the Northridge earthquake. In the conventional strength-designed structure largest amount of seismic input energy is dissipated by the inherent damping which is assumed to be 5% of the critical damping, and significant amount of energy is dissipated by inelastic deformation of the chord members. In addition

small portion of the dissipated energy is from yielding of some vertical members in the lower story staggered trusses. In the structure with friction dampers about 40% of the dissipated energy is from activation of the friction dampers and no energy is dissipated by the other structural elements. This indicates that, after occurrence of a design level earthquake, the structure with dampers may be reused after replacement of damaged dampers and minor repair of nonstructural components while major retrofit or complete demolition may be required in the structure without dampers. Fig. 16 shows the hysteresis curve of a friction damper located at the end of the chord member in the second story obtained from the Northridge earthquake. It can be observed that during the earthquake the damper experiences repeated yielding, dissipating large hysteretic energy. The seismic energy dissipated by the specific damper during the Northridge ground motion is estimated to be 11,964 kN cm.

4. Seismic safety of the model structures

4.1. Collapse margin ratios of the model structures

In this section the statistical seismic performance evaluation procedure proposed in the FEMA P695 [25] is applied to the model structures, which proposes a methodology for quantifying building system performance and response parameters for use in seismic design. In this approach nonlinear incremental dynamic analyses are conducted to establish the median collapse capacity and collapse margin ratio (CMR) for the analysis models. The ratio between the median collapse intensity, S_{CT} , and the MCE (maximum considered earthquake) inten-

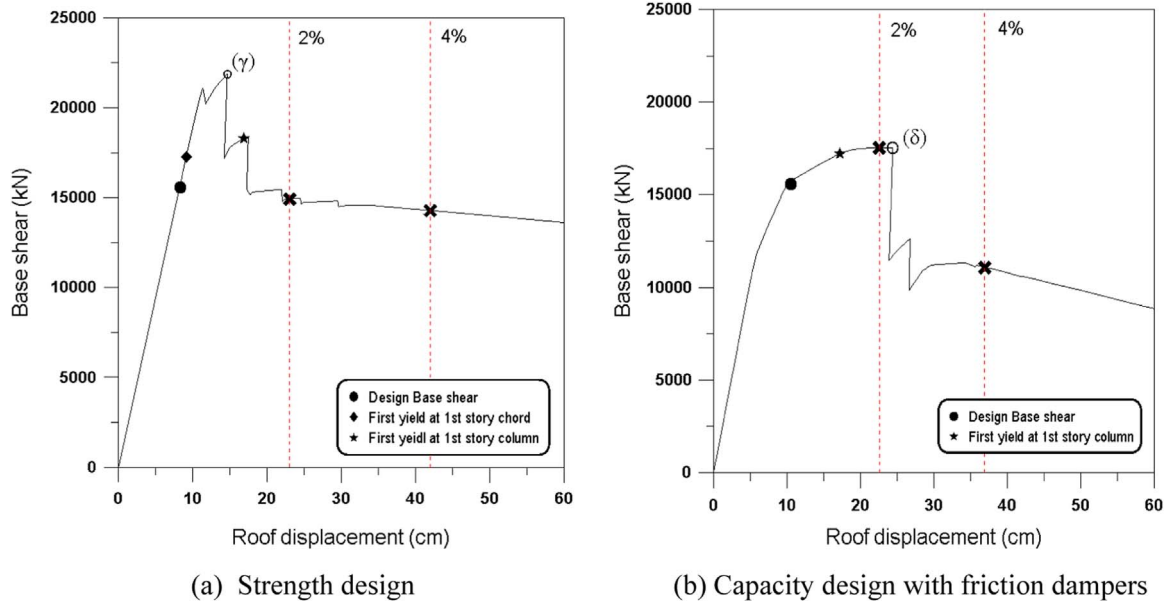


Fig. 10. Pushover curves of the 12-story structures. (a) Strength design, and (b) Capacity design with friction dampers.

sity, S_{MT} , is defined as the collapse margin ratio (CMR). The adjusted collapse margin ratio (ACMR) is obtained by multiplying the tabulated spectral shape factor with the collapse margin ratio that is predicted using the Far-Field record set. Acceptable values of adjusted collapse margin ratio are based on total system collapse uncertainty, β_{TOT} , and established values of acceptable probabilities of collapse. They are based on the assumption that the distribution of collapse level spectral intensities is lognormal, with a median value, S_{CT} , and a lognormal standard deviation equal to the total system collapse uncertainty, β_{TOT} .

$$\beta_{TOT} = \sqrt{\beta_{RTR}^2 + \beta_{DR}^2 + \beta_{TD}^2 + \beta_{MDL}^2} \quad (10)$$

The total system collapse uncertainty is a function of record-to-record (RTR) uncertainty, design requirements related (DR) uncertainty, test data-related (TD) uncertainty, and modeling (MDL) uncertainty. The values of total system collapse uncertainty, β_{TOT} , and the acceptable values of adjusted collapse margin ratio, $ACMR_{20\%}$, are provided in the FEMA P695.

To evaluate the seismic performance of the model structures

Table 3
Earthquake record used for non-linear dynamic analysis.

Name	M	Year	PGA (g)	PGV (cm/s.)
Northridge	6.7	1994	0.52	63
Imperial Valley	6.5	1979	0.38	42
Kobe, Japan	6.9	1995	0.51	37
Kocaeli, Turkey	7.5	1999	0.36	59
Manjil, Iran	7.4	1990	0.51	54
Supersition Hills	6.5	1987	0.45	36
San Fernando	6.6	1971	0.21	19

following the FEMA P695 process, the over-strength factor and the period-based ductility of the model structures are computed first from pushover analysis and are presented in Table 4. Then incremental dynamic analyses of the model structures are carried out using the twenty two pairs of scaled far-field records provided by the PEER NGA Database [22]. They are scaled in such a way that the spectral acceleration of each record at the fundamental period of the structure

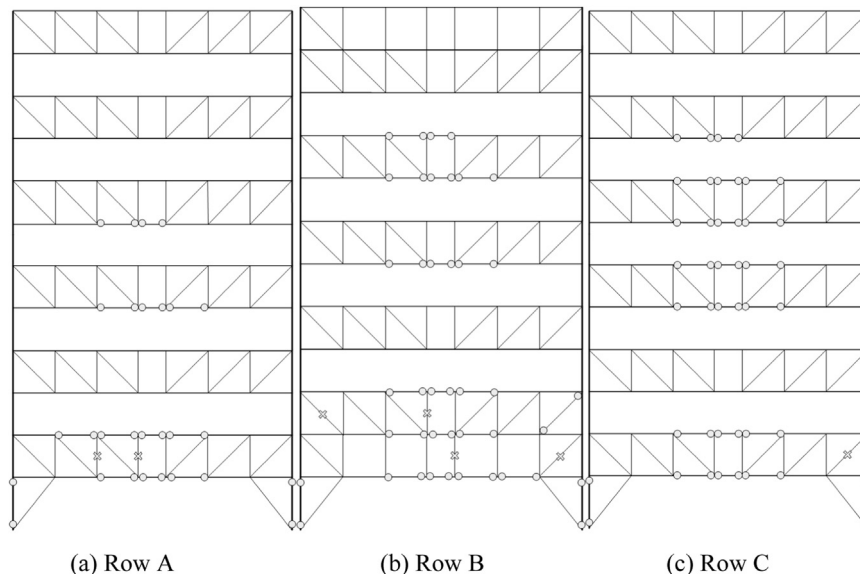


Fig. 11. Plastic hinge formation of the 12-story structure (Strength design). (a) Row A, (b) Row B, and (c) Row C.

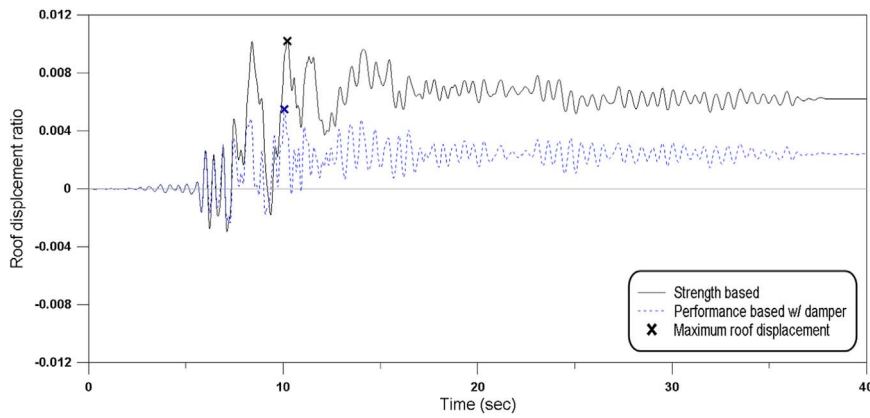


Fig. 12. Roof displacement time histories of the 6-story model structures subjected to the Imperial Valley earthquake.

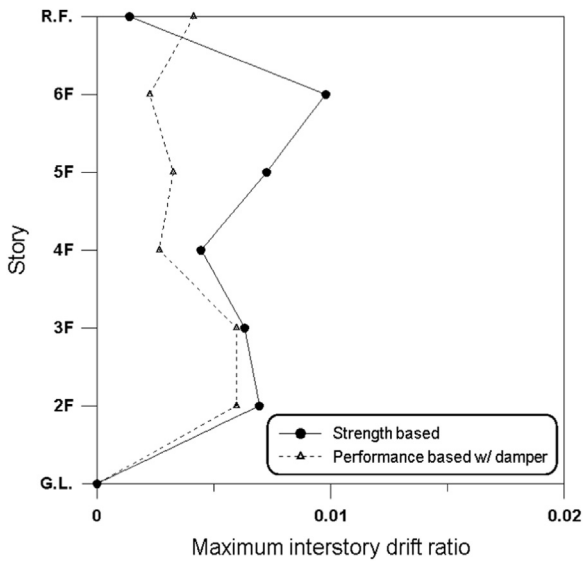


Fig. 13. Mean maximum inter-story drifts of the model structures obtained from nonlinear dynamic analyses using seven earthquake records.

is equal to that of the design spectrum. Damping ratios of 5% are used for all vibration modes, and the spectral acceleration vs. maximum inter-story drift ratio is plotted. Figs. 17 and 18 depict the incremental dynamic analysis results of the 6- and the 12-story model structures, respectively, obtained using 44 earthquake records. The collapse margin ratios (CMR) of the model structures are determined from the spectral accelerations at which dynamic instability of the structures occurs for more than 22 earthquake records. The dynamic instability is defined as the point at which the stiffness starts to decrease less than 20% of the initial stiffness. In this study the total system collapse uncertainty is evaluated as 0.7 in accordance with Table 7-2 of FEMA

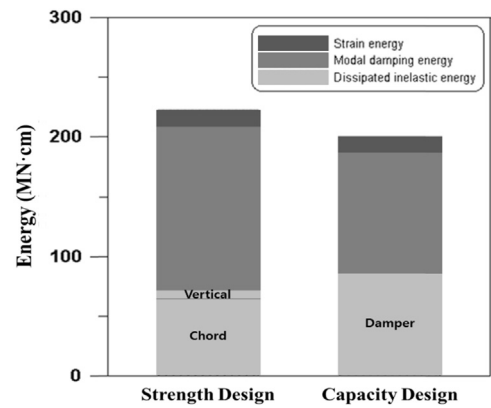


Fig. 15. Dissipated energy in the 6-story model structures during Northridge earthquake.

P695 based on the assumption that the modeling uncertainty is Good, the test data-related uncertainty is Poor, and the design requirements related uncertainty is Good. Table 5 summarizes the analysis results, which shows that the adjusted collapse margin ratios of all model structures are larger than the acceptable values of *ACMR* 20% provided in the FEMA P695. This implies that the parameters used in the seismic design of the model structures are valid. It also can be noticed that the collapse margins of the model structures designed with friction dampers are significantly larger than those of the strength-designed structures without dampers.

4.2. Fragility analysis

The seismic fragility is described by the conditional probability that the structural capacity, *C*, fails to resist the structural demand, *D*, given the seismic intensity hazard, *SI*, and is modeled by a lognormal cumulative distribution function as follows [26]:

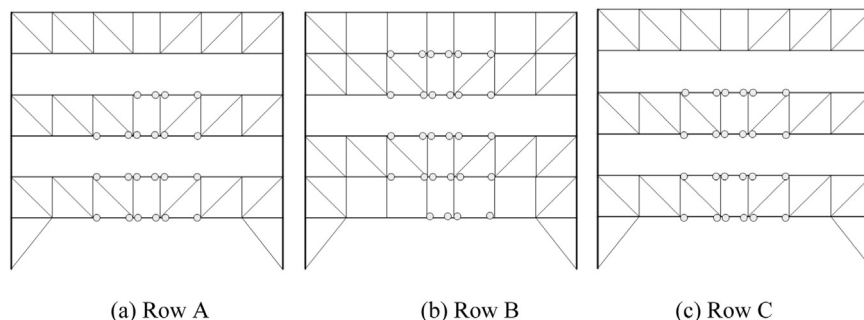


Fig. 14. Plastic hinge formation in the strength-designed 6-story structure obtained from nonlinear dynamic analysis using the Northridge earthquake record. (a) Row A, (b) Row B, and (c) Row C.

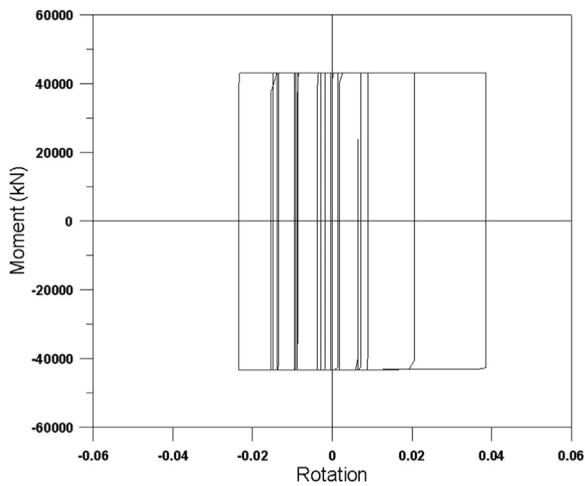


Fig. 16. Hysteresis loop of a friction damper during Northridge earthquake.

Table 4
Overstrength factor (Ω) and period-based ductility (μ_T) of the model structures.

Model		Ω	μ_T
6F	Strength based	1.539	1.725
	Performance based w/ dampers	1.422	4.778
12F	Strength based	1.407	1.188
	Performance based w/ dampers	1.016	2.920

$$P[D \geq C] = \Phi(\ln[D/\hat{C}]/\beta_c) \quad (11)$$

where $\Phi[\cdot]$ = standard normal probability integral, \hat{C} = median structural capacity, associated with the limit state, and β_c = uncertainty in C . Table 4 shows the median structural capacity \hat{C} associated with the four limit states obtained from the incremental dynamic analysis results of the 44 earthquake records. Fragility analyses are carried out for the ‘Complete damage’ state defined as the maximum displacement at which the strength decreased to 80% of the maximum strength in the pushover curve. Fig. 19 depicts the fragility curves of the analysis model structures, where it can be observed that the structures designed with friction dampers have significantly lower probability of reaching the collapse state than the strength-designed structures. FEMA P695

requires that the probability of failure of a structure subjected to the MCE (maximum considered earthquake) level earthquake, which is 3/2 of the design level earthquake, be smaller than 0.1 in order for the seismic design variables used for the model structures to be valid. It can be observed in the fragility curves that the failure probabilities of all the 6-story structures are smaller than 0.1, whereas that of the strength-designed conventional 12-story structure is almost 1.0.

5. Seismic performance of the model structures designed with higher R factor

As stated before, currently no specific value of response modification factor is assigned for staggered truss systems in design codes. The fragility analysis presented in the previous section shows that the staggered truss systems designed with the response modification factor of 3, especially the capacity-designed structures with friction dampers, have enough margin for safety against the design level seismic load. In this section the seismic performance of the model structures designed with higher R factor of 6 is investigated. This study is motivated by the fact that in ASCE 7-13 significantly higher R factor of 7 is assigned to the steel special truss moment frames with special segments which have similarity in shape with staggered truss systems. To investigate the validity of the higher R factor used for seismic design, the same analysis process specified in the FEMA P-695 is followed.

Fig. 20 depicts the pushover curves of the model structures designed with $R=6$. In comparison with the pushover analysis results of the structures designed with R factor of 3, the overall strengths of the model structures are significantly reduced due mainly to the reduced seismic design base shear. The over-strength factors and the period-based ductility factors of the model structures designed with $R=6$ are obtained from the pushover curves and are presented in Table 6. In the 6-story structures no significant change can be observed both in the over-strength and the ductility factors compared with those of the structures designed with $R=3$. In the 12-story structures both factors slightly increased compared with those of the structures designed with $R=3$. The independency of the over-strength factors on the R factor is due to the fact that both the maximum strength and the design base shear due decrease in almost the same proportion.

Figs. 21 and 22 depict the incremental dynamic analysis results of the 6- and the 12-story structures designed with $R=6$, respectively. It can be observed that the inter-story drift ratios corresponding to a given

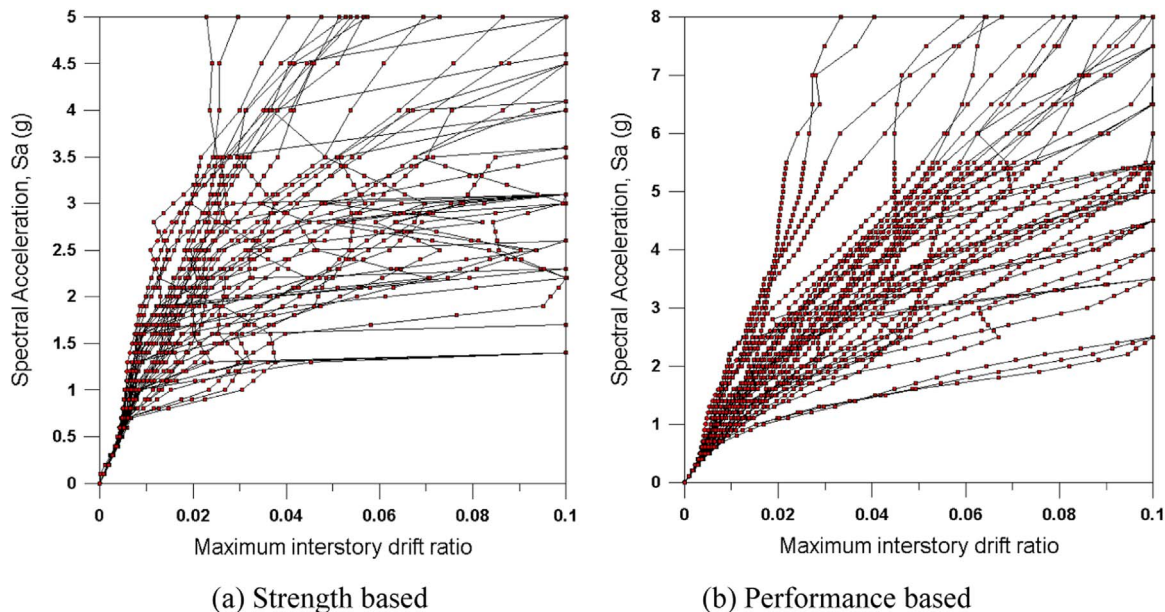


Fig. 17. Incremental dynamic analysis results of 6-story structures. (a) Strength based, and (b) Performance based.

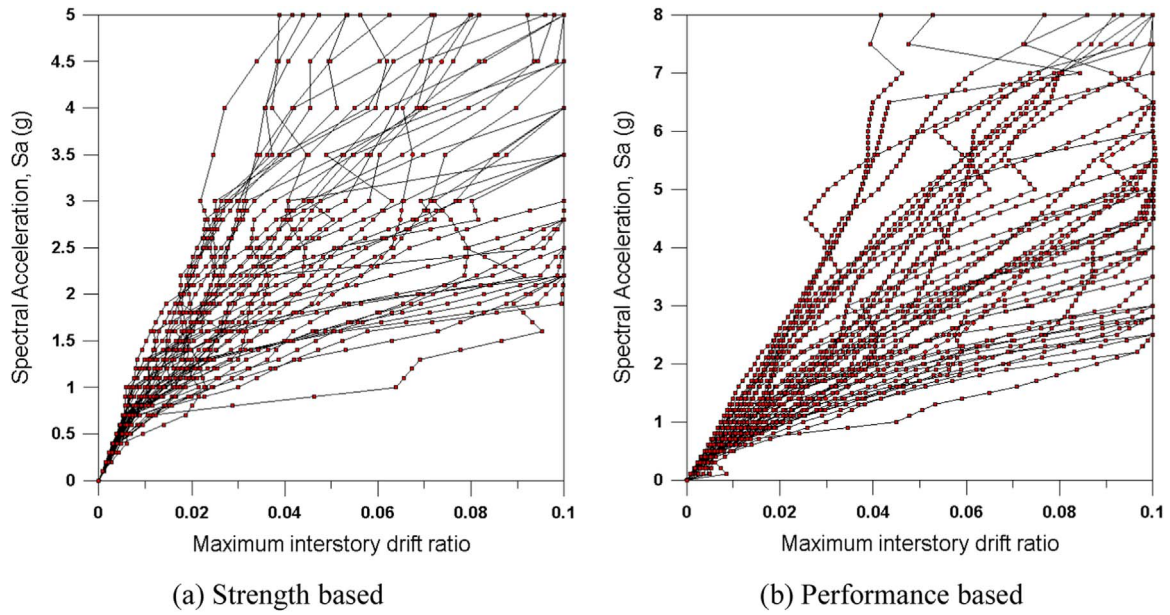


Fig. 18. Incremental dynamic analysis results of 12-story structures. (a) Strength based, and (b) Performance based.

Table 5
Parameters for evaluation of seismic safety of model structures.

(a) 6-story								
	\widehat{S}_{CT}	S_{MT}	CMR	SSF	ACMR	β_{TOT}	ACMR _{20%}	Pass/Fail
Strength based	3.5	1.5	2.333	1.120	2.613	0.7	1.80	Pass
Performance based	7.0	1.5	4.667	1.245	5.812	0.7	1.80	Pass
(b) 12-story								
	\widehat{S}_{CT}	S_{MT}	CMR	SSF	ACMR	β_{TOT}	ACMR _{20%}	Pass/Fail
Strength based	3.0	1.176	2.551	1.072	2.735	0.7	1.80	Pass
Performance based	6.5	1.169	5.560	1.211	6.734	0.7	1.80	Pass

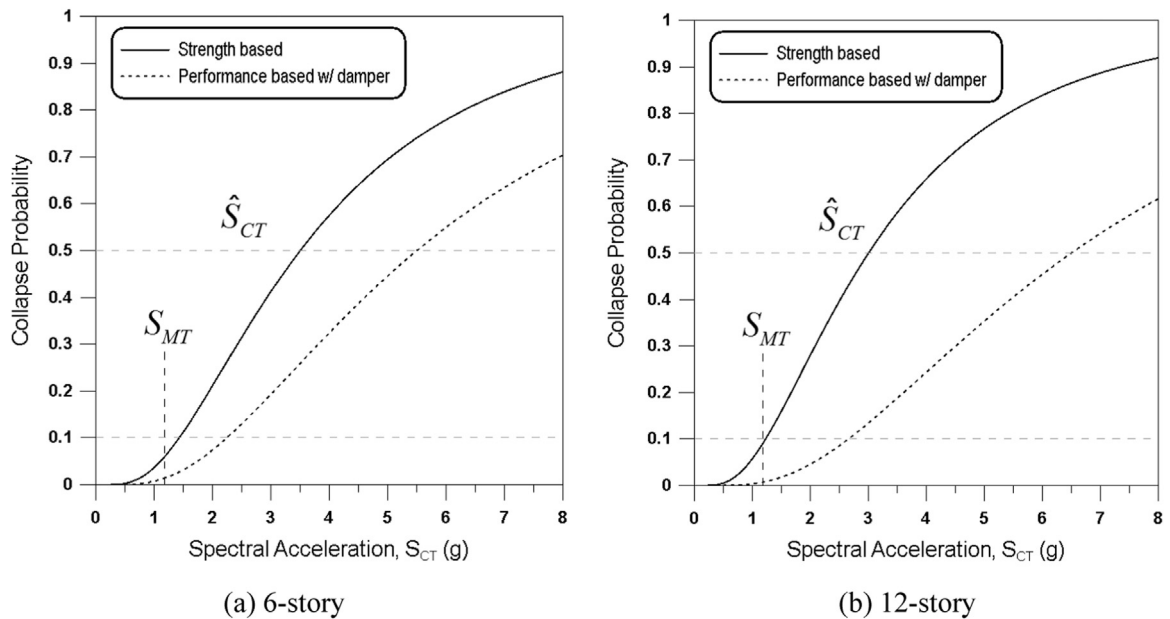


Fig. 19. Fragility curves of the analysis model structures. (a) 6-story, and (b) 12-story.

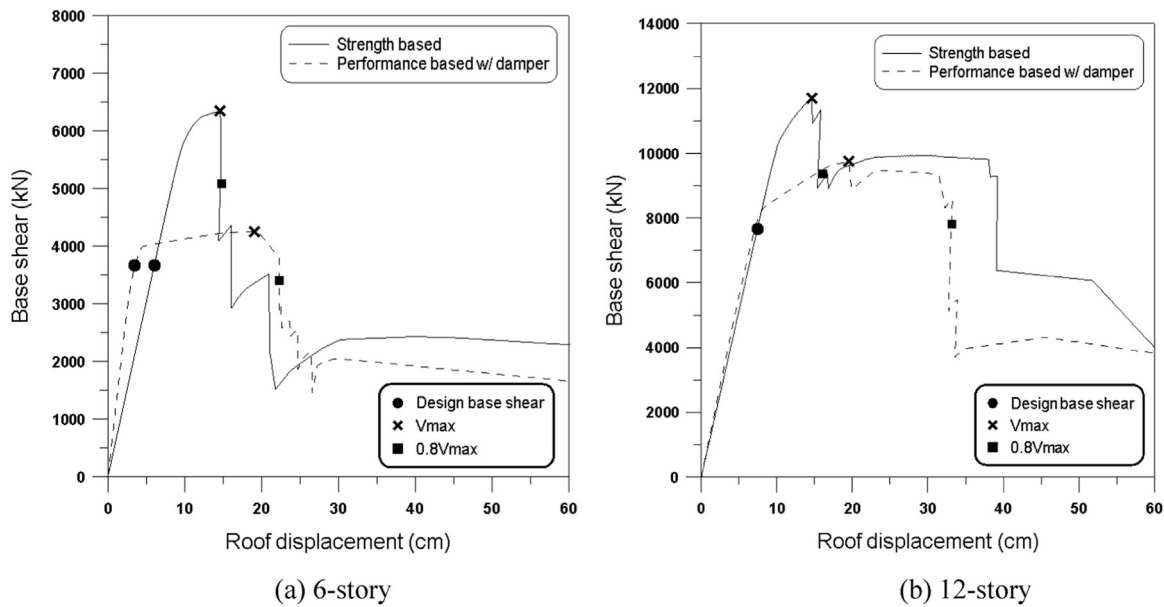


Fig. 20. Pushover curves of the model structures designed with R=6. (a) 6-story (b) 12-story.

Table 6
Overstrength factor (Ω) and period-based ductility (μ_T) of the model structures designed with R=6.

	Model	Ω	μ_T
6-story	Strength based	1.732	1.305
	Performance based w/ damper	1.159	5.444
12-story	Strength based	1.526	1.345
	Performance based w/ damper	1.272	3.523

spectral acceleration are generally larger than those obtained from analysis of the structure designed with R=3. Table 7 shows the parameters for evaluation of seismic safety of model structures designed with R=6. Compared with those of the structures designed with R=3, the ACMR of the 6-story strength- and capacity-designed structures is reduced by 27% and 48%, respectively. In the 12-story structures the reduction is 9% and 35%, respectively. It can be observed that the

ACMR values of the structures designed with R=6 are still larger than the $ACMR_{20\%}$ specified in the FEMA P695. However the ACMR of the 6-story structure is quite close to the specified value, which implies that the margin for safety is very small. Fig. 23 shows the fragility curves of the analysis model structures designed with R=6. Compared with the results of the structures designed with R=3 shown in Fig. 19, the failure probabilities of the structures designed with R=6 are generally increased. It also can be observed that the structures designed with friction dampers have lower probability of reaching the collapse state than the structures without dampers. The failure probabilities of the structures without dampers subjected to the MCE level earthquake turn out to be higher than 0.1, which implies that the response modification factor used for seismic design of the model structures is not valid. However the failure probabilities of the structures designed with dampers still remain smaller than 0.1. This observation supports the possibility of using higher R factor for structures installed with energy dissipation devices.

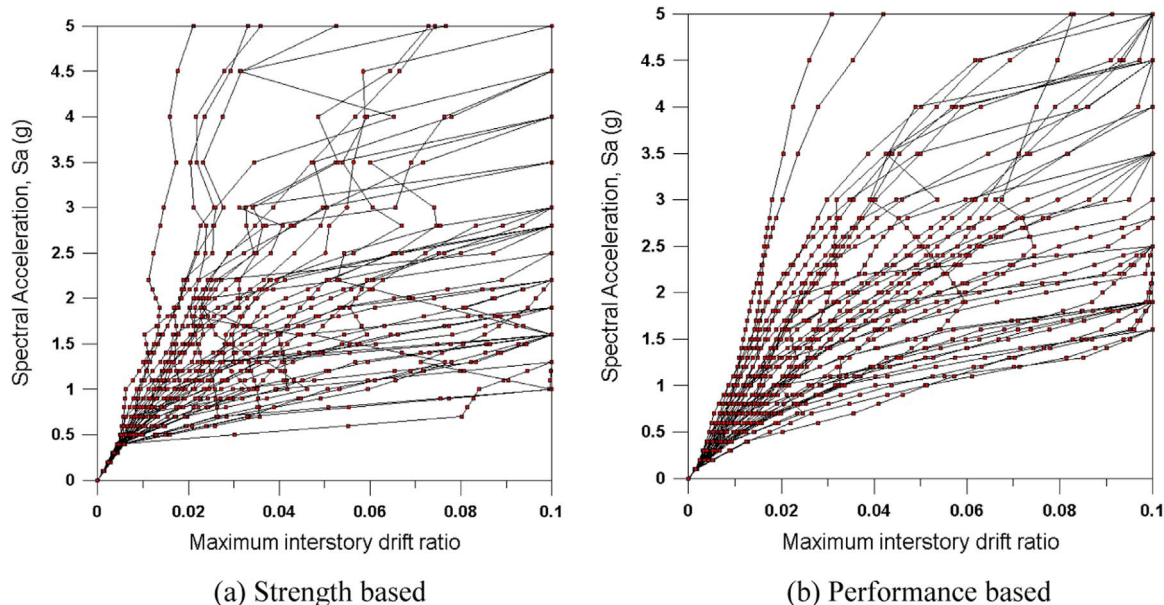


Fig. 21. Incremental dynamic analysis results of 6-story structures designed with R=6. (a) Strength based, and (b) Performance based.

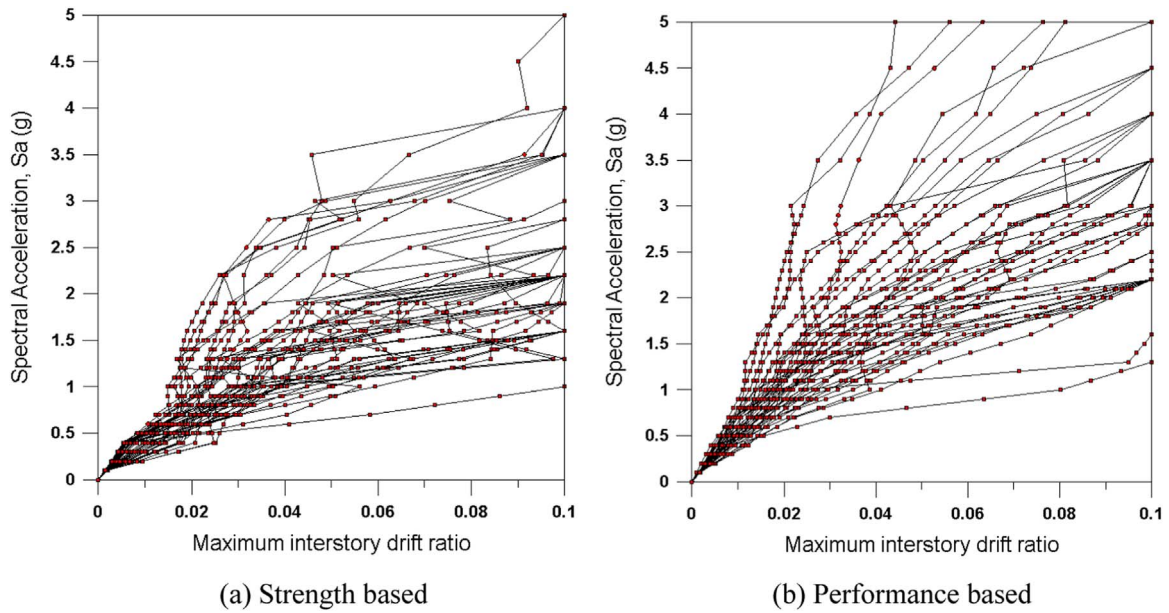


Fig. 22. Incremental dynamic analysis results of 12-story structures designed with R=6. (a) Strength based, and (b) Performance based.

Table 7

Parameters for evaluation of seismic safety of model structures designed with R=6.

(a) 6-story								
	\widehat{S}_{CT}	S_{MT}	CMR	SSF	ACMR	β_{TOT}	ACMR _{20%}	Pass/Fail
Strength based	2.2	1.253	1.756	1.086	1.908	0.7	1.80	Pass
Performance based w/ damper	2.8	1.219	2.297	1.311	3.011	0.7	1.80	Pass
(b) 12-story								
	\widehat{S}_{CT}	S_{MT}	CMR	SSF	ACMR	β_{TOT}	ACMR _{20%}	Pass/Fail
Strength based	1.9	0.847	2.242	1.111	2.490	0.7	1.80	Pass
Performance based w/ damper	3.0	0.882	3.400	1.285	4.368	0.7	1.80	Pass

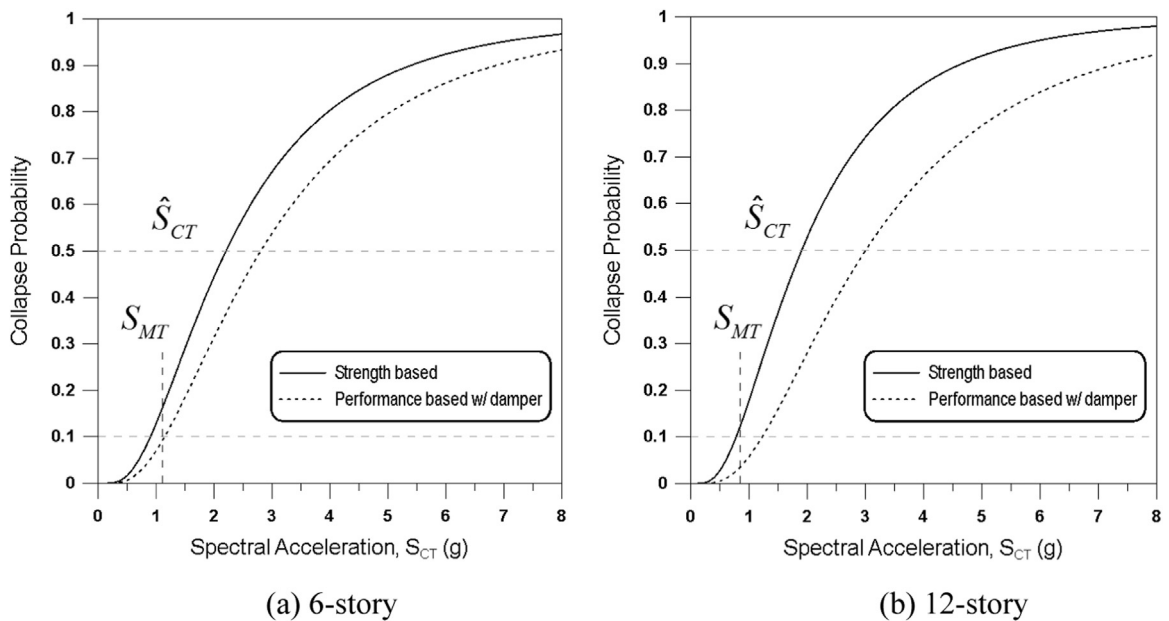


Fig. 23. Fragility curves of the analysis model structures designed with R=6. (a) 6-story, and (b) 12-story.

6. Conclusions

In this study the seismic performance of staggered truss system structures with friction dampers in the vierendeel panels was evaluated. To this end 6- and 12-story structures with friction dampers were designed based on the capacity design procedure. For comparison the same structures without dampers were designed following the strength based approach specified in the ASCE 7-13, and the seismic performances of all model structures were compared. Fragility analyses were carried out to evaluate the seismic safety of the model structures and to validate the response modification factor used for seismic design.

According to the analysis results the plastic design method combined with the capacity design approach led to the formation of plastic hinges mainly at vierendeel panels when subjected to a seismic load. It was observed that the substitution of rotational friction dampers at the location of plastic hinges resulted in reduced overall strength but enhanced ductility and reduced probability of failure when the structures were subjected to design level seismic load. The application of the FEMA P695 process showed that the failure probabilities of the model structures designed using $R=3$ were small enough to ensure safety against MCE level earthquakes. However the same structures designed with $R=6$ failed to satisfy the safety requirement when designed following code-based procedure without friction dampers. Even in this case the seismic safety turned out to be enhanced to the level of safety when friction dampers were used in the chord members of the vierendeel panels.

Acknowledgements

This research was financially supported by the Ministry of Trade, Industry and Energy(MOTIE) and Korea Institute for Advancement of Technology(KIAT) through the China-Korea Cooperative R & D program.

References

- [1] M.P. Cohen, Design solutions utilizing the staggered-steel truss system, AISC Eng. J. (1986) Third quarter.
- [2] B.S. Pollak, M. Gustafson, Complex Apartments, Modern Steel Construction, American Institute of Steel Construction, Fall, 2004.
- [3] J. Kim, J. Lee, Y. Kim, Inelastic behavior of staggered truss systems, Struct. Des. Tall Spec. Struct. 16 (1) (2007) 85–105.
- [4] X.H. Zhou, Y.J. He, L. Xu, Q.S. Zhou, Experimental study and numerical analyses on seismic behaviors of staggered-truss system under low cyclic loading, Thin Walled Struct. 47 (11) (2009) 1343–1353.
- [5] C.K. Chen, W. Zhang, Experimental study of the mechanical behavior of steel staggered truss system under pool fire conditions, Thin Walled Struct. 49 (11) (2011) 1442–1451.
- [6] C.K. Chen, D. Zhang, W. Zhang, B. Shen, Experimental behaviors of steel staggered truss system exposed to fire under lateral force, Int. J. Steel Struct. 12 (1) (2012) 59–70.
- [7] J. Kim, J. Lee, B. Kim, Seismic retrofit schemes for staggered truss structures, Eng. Struct. 102 (2015) 93–107.
- [8] J. Kim, Y. Jun, H. Kang, Seismic behavior factors of rc staggered wall buildings, Int. J. Concr. Struct. Mater. 10 (3) (2016) 355–371.
- [9] FEMA 450, NEHRP Recommended Provisions for Seismic Regulations for New Buildings and Other Structures, The Building Seismic Safety Council, Washington, D.C., 2003.
- [10] AISC, Steel Design Guide 14: Staggered Truss Framing Systems, American Institute of Steel Construction, Chicago, 2003.
- [11] B.G. Morgen, Y.C. Kurama, Seismic response evaluation of posttensioned precast concrete frames with friction dampers, J. Struct. Eng. 134 (1) (2008) 132–145.
- [12] H. Chung, B. Moon, S. Lee, J. Park, K. Min, Seismic performance of friction dampers using flexure of rc shear wall system, Struct. Des. Tall Spec. Build. 18 (2009) 807–822.
- [13] I.H. Mualla, E.D. Jakupsson, L.O. Nielsen, Structural behavior of 5000 kN damper, in: Proceedings of the European Conference on Earthquake Engineering, ECEE, Ohrid, Macedonia, 2010.
- [14] K. Mizutani, K. Hirakawa, M. Nakashima, Construction of 300 m Vertical City ABENO HARUKAS, International Journal of High-Rise Buildings, Accepted for publication, 2015.
- [15] Damptech. Friction Dampers-Capacities and Dimensions, <<http://www.damptech.com/download.html>>, 2015
- [16] H. Dai, Z. Liu, W. Wang, Structural passive control on electromagnetic friction energy dissipation device, Thin-Walled Struct. 58 (2012) 1–8.
- [17] ASCE, Minimum Design Loads for Buildings and Other Structures, ASCE/SEI 7-13, American Society of Civil Engineers, Virginia, 2013.
- [18] AISC, Specification for Structural Steel Buildings, AISC 360-16, American Institute of Steel Construction, Chicago, Illinois, 2016.
- [19] S.-H. Chao, S.C. Goel, Performance-Based Plastic Design of Seismic Resistant Special Truss Moment Frames, Report No. UMCEE 06-03, Department of Civil and Environmental Engineering, University of Michigan, Ann Arbor, MI, 2006.
- [20] AISC, Seismic Provisions for Structural Steel Buildings, AISC 341-10, American Institute of Steel Construction, Chicago, Illinois, 2010.
- [21] ASCE, Seismic Evaluation and Retrofit of Existing Buildings, ASCE/SEI 41-13, American Society of Civil Engineers, Virginia, 2014.
- [22] S. Wu, S. Lee, L. Chung, Cyclic loading test of rotation type friction damper. in: Proceeding of the Spring Conference of Korea Institute of Sound and Vibration, 2009.
- [23] PERFORM-3D. Nonlinear analysis and Performance Assessment for 3D Structures-User Guide. Berkeley (CA, USA): Computers and Structures, 2006.
- [24] PEER, PEER NGA Database, Pacific Earthquake Engineering Research Center, University of California, Berkeley, U.S.A, 2006 <<http://peer.berkeley.edu/nga/>>.
- [25] FEMA, Quantification of Building Seismic Performance Factors, Report No. FEMA P695, Federal Emergency Management Agency, Washington DC, 2009.
- [26] C.A. Cornell, F. Jalayer, R. Hamburger, D. Foutch, Probabilistic Basis for 2000 SAC federal emergency management agency steel moment frame guidelines, J. Struct. Eng. (2002).
- [27] MIDAS-Gen, MIDAS SDS, General Structure Design System for Window, Version 3.4.0, 2016.